



# Amplification of a radially polarized beam in a thermally guiding ytterbium-doped fiber rod

T. L. Jefferson-Brain<sup>1</sup> · C. R. Smith<sup>1</sup> · M. D. Burns<sup>1</sup> · P. C. Shardlow<sup>1</sup> · W. A. Clarkson<sup>1</sup>

Received: 11 June 2019 / Accepted: 2 August 2019 / Published online: 14 August 2019  
© The Author(s) 2019

## Abstract

Amplification of a radially polarized beam from an Yb:YAG seed laser at 1030 nm in a very-large-core triple-clad ytterbium-doped fiber configured as a thermally guiding fiber rod amplifier is demonstrated. The amplifier yielded a maximum output power of 10.7 W (limited by available pump power) with corresponding single-pass gain of 6.4 dB, while the radial polarization purity was maintained over the full range of pump power with a measured polarization extinction ratio of 100:1. The amplified output beam displayed the characteristic donut-shaped intensity profile with negligible beam distortion as evidenced by a measured beam propagation factor ( $M^2$ ) of  $2.1 \pm 0.1$ . A simplified model for propagation of a radially polarized beam in a thermally guided fiber rod is developed to provide insight into the underlying design principles and to establish a strategy for scaling output power. The power scaling limitations of this approach are considered.

## 1 Introduction

Cylindrical vector beams with radial polarization have attracted growing interest over the last decade stimulated by numerous applications. Radially polarized beams are characterized by an electric field direction that is aligned with the radius vector at all points across the transverse profile. To avoid a central discontinuity, this polarization state requires a central intensity minimum, and hence leading to a ‘donut’-like appearance. Their unique properties have found application in a number of areas including particle manipulation [1], high resolution imaging [2], and laser processing of material [3, 4]. The potential benefits that radially polarized beams offer can be very dramatic, depending on the particulars of the application. For example, in laser fusion cutting of metals, cutting speeds a factor of 1.5–2 times faster than traditional unpolarized (or uniformly polarized) beams along with which improved surface finish quality can be attained. The underlying advantage of radially polarized beams in laser cutting is derived from their global p-polarization relative to the cutting front (kerf) which leads to superior absorption over the cut front for a range of angles of incidence and, due to the axially symmetric nature of the

beam, is independent of cutting direction [4]. Not surprisingly, there has been much activity directed toward improving techniques for generating radially polarized beams and especially scaling power to meet the needs of demanding applications such as laser cutting.

Current methods of generating radial polarization include the use of intra-cavity elements such as birefringent crystals [5, 6], grating mirrors [7], and spatially variant waveplates [8] for direct generation in a laser resonator. Alternatively, there are schemes for external conversion to radial polarization starting from more easily achieved laser modes, such as interferometers [9] or segmented waveplates [10]. At present, these techniques all suffer from the shortcomings of limited power scalability and/or issues relating to purity. An alternative strategy is to start with a high-purity low-power radially polarized source and then scale-up power using an amplifier. This approach has the appeal that it decouples the issues of radial polarization selection from power scaling. Amplification of radially polarized beams in rod [11], slab [12], and thin-disk [13] gain medium geometries has been demonstrated, but with limited success owing to thermal effects or the need for complicated multi-pass architectures. Cladding-pumped fiber amplifiers have also been investigated in this context offering the potential for high power, high gain, and immunity from detrimental thermal effects [14]. However, mode purity and stability issues associated with mode coupling between degenerate (or nearly degenerate) modes have so far rendered this approach unreliable.

✉ T. L. Jefferson-Brain  
t.jefferson-brain@soton.ac.uk

<sup>1</sup> Optoelectronics Research Centre, University of Southampton, Southampton SO17 1BJ, UK

In this paper, we explore a different approach based on an amplifier geometry that lies between conventional rod and fiber amplifier geometries. The geometry, which we refer to as the thermally guiding fiber rod (TGFR) amplifier, has been explored before in the context of amplifying fundamental ( $TEM_{00}$ ) modes with promising results [15]. The underlying design philosophy underpinning the TGFR geometry is to exploit thermal effects in the form of relatively weak thermal guiding to yield a much larger guided mode size than would be the case for conventional large mode area fibers in a relatively short ( $\sim 10$ – $100$  cm) length of gain medium. In this way, the TGFR effectively combines the beneficial properties of bulk and fiber gain media having a large surface-to-volume ratio for effective thermal management and relative immunity from detrimental thermal effects. Moreover, the large mode area benefits energy storage and greatly assists in the avoidance of optical damage and suppression of non-linear processes that plague fiber geometries in some regimes of operation. These properties make the TGFR gain medium geometry an attractive candidate for the amplification of pulsed sources and, due to its cylindrical symmetry, more exotic axially symmetric modes such as radially polarized modes. The geometry of the TGFR means that thermally induced stresses can result in birefringence between radial and azimuthal polarization components; an effect which can cause depolarization in beams with polarization components in both radial and azimuthal directions [16]. Therefore, it was theorized that a purely radially polarized beam could be amplified without depolarization in the TGFR.

Here, we demonstrate amplification of a high-purity radially polarized mode in a TGFR amplifier by 6.4 dB to 10.7 W at 1030 nm maintaining beam quality and

polarization purity. Moreover, we show that this amplifier geometry has the potential for scaling to much higher powers in the multi-hundred-watt regime and beyond.

The paper is organized as follows: Sect. 2 describes the radially polarized Yb:YAG seed laser used in our experiments. Section 3 describes the TGFR design and presents a theoretical model for analyzing the propagation of higher-order modes through the core of the fiber rod. This is applied to the case of a radially polarized mode to provide insight into experimental design and to inform future power scaling considerations. Section 4 discusses the experimental setup for the TGFR amplifier and presents the results for performance. Finally, Sect. 5 considers the potential for further power scaling of the radially polarized beams using a TGFR amplifier geometry and presents the overall conclusions.

## 2 Radially polarized seed source

A radially polarized Yb:YAG laser was developed to provide the seed beam for amplification experiments with the TGFR. The seed laser (shown in Fig. 1) employed a simple two-mirror resonator design with feedback for lasing provided by a convex pump in-coupling mirror (10 cm radius of curvature) with high reflectivity ( $> 99.8\%$ ) at the lasing wavelength (1030 nm) and high transmission ( $> 98\%$ ) at the pump wavelength ( $\sim 940$  nm), and a plane output coupler with 96% reflectivity at 1030 nm. The Yb:YAG gain medium had a diameter of 2 mm, length of 3 mm, and an  $Yb^{3+}$  doping concentration of 7.5 at.%. The latter was mounted in a water-cooled copper heat sink and located in close proximity to the pump in-coupling mirror. Pump light was provided by a commercial fiber-coupled 940 nm diode laser (nLight,

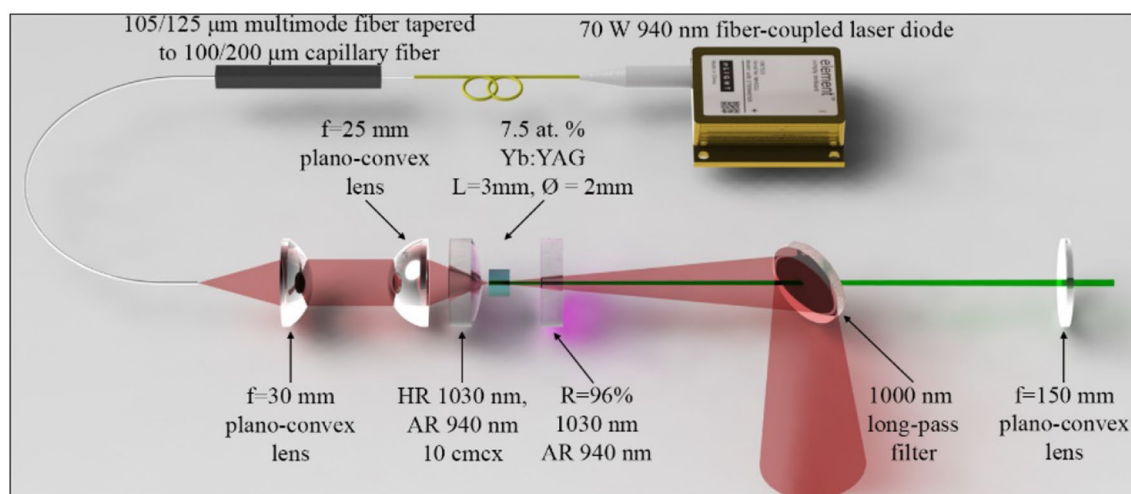


**Fig. 1** Schematic of the end-pumped 1030 nm radially polarized Yb:YAG laser used as a seed source for the thermally guiding fiber rod amplifier

Inc.) with a 105  $\mu\text{m}$  diameter core with a 0.22 NA. The pump delivery fiber was spliced to a capillary fiber with an inner air-hole diameter of 100  $\mu\text{m}$  and outer diameter 200  $\mu\text{m}$  via a section of the fiber tapered to a solid core. The taper transfers the pump light into the ring of the glass capillary to provide an annular near-field pump profile at the output of the capillary fiber. The latter was then relay imaged into the center of the Yb:YAG crystal using pair of plano-convex lenses with 30 mm and 25.4 mm focal lengths, yielding a pump spot diameter of 169  $\mu\text{m}$  with a 72  $\mu\text{m}$  central hole. In this way, the pump spot inside the Yb:YAG crystal matches the desired intensity profile of the targeted radially polarized mode [5] favoring this mode over the fundamental ( $\text{TEM}_{00}$ ) mode and higher-order modes. The choice of a relatively short Yb:YAG crystal and high doping level ensures that the annular-shaped beam is maintained over the pumped region, maximizing discrimination against unwanted transverse modes.

Thermally induced bifocusing in the Yb:YAG was used to discriminate between the radially polarized mode and azimuthally polarized mode and other uniformly polarized modes (e.g.,  $\text{LG}_{01}$  mode) with the same donut-shaped intensity profile [17]. This approach exploits the different thermal lens focal lengths for radial and azimuthal polarizations with a resonator design that is stable for the radially polarized mode, but unstable for the azimuthally polarized mode. This selective instability was achieved using a convex pump in-coupling mirror with -100 mm radius of curvature. The cavity mirror separation was 15 mm, mandated by the calculated thermal lens focal length required to achieve the required stability condition and optimum mode overlap with the inversion profile. Due to the nature of the design, the radially polarized source had a range of operation between absorbed pump powers of 25 and 33 W. At lower pump power, lasing was suppressed by virtue of the cavity being unstable for both radial and azimuthal polarization. At high pump powers, the radially polarized output beam became degraded by thermally induced lens aberration.

The radial polarization purity was quantified by measuring the two-lobe intensity profile contrast after transmission through a linear polarizer as a function of angle of

the polarizer [8, 12]. Intensity values were sampled from CCD camera images in a circular path with a radius chosen such that the circular path crosses the intensity maxima of the two-lobe profile (see Fig. 2). From this, the ratio of the maximum and minimum transmitted intensity is calculated and then averaged over all orientations of the polarizer to determine the radial polarization extinction ratio (RPER). In our case, the intensity profiles were examined for 36 different polarizer orientations. At the optimum operational pump power of 26 W, the measured RPER was 100:1, the output power was 2.5 W, the spot size was 140  $\mu\text{m}$ , and the beam divergence half-angle was measured to be 4.5 mrad. The high polarization purity was complimented by a measured  $M^2$  parameter of  $1.9 \pm 0.1$ , agreeing closely with the minimum theoretical  $M^2$  parameter of 2.0.

### 3 The thermally guiding fiber rod amplifier

The TGFR employed in our experiments was based on a commercially available triple-clad fiber (Nufern) with a very large Yb-doped core of diameter, 300  $\mu\text{m}$  and 0.11 NA. The latter was surrounded by an octagonal inner cladding with a flat-to-flat distance of 400  $\mu\text{m}$  and an NA of 0.22, and finally, a 480- $\mu\text{m}$ -diameter circular outer cladding (see Fig. 3). This fiber was selected due to its extremely large, uniform, Yb-doped core and could be employed in either core or cladding-pumped configurations.

An important prerequisite for operating this fiber as a TGFR amplifier for a radially polarized beam is careful

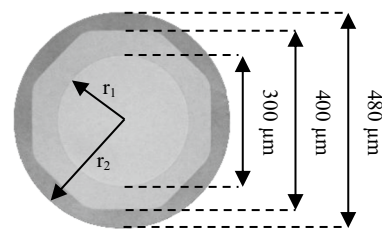
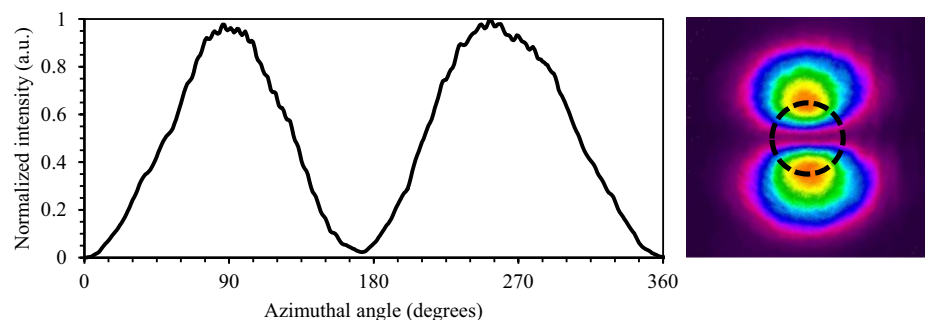


**Fig. 3** Cross-sectional view of the Yb-doped fiber used in TGFR amplifier experiments

**Fig. 2** Example of one of the 36 data sets used for the calculation of the radial polarization extinction ratio for the seed source. Normalized intensity sampled from an image (right) is plotted against azimuthal angle. The inset image has a dashed line representing the circular path over which the intensity data were sampled



selection of the operating parameters (i.e., pump power, input beam size, and fiber rod length) to ensure thermal guidance over the full length of the fiber rod while avoiding interaction of the beam with the boundary between the core and inner cladding, which would lead to mode coupling and beam distortion. For this reason, we have developed a simple model for thermal guidance of a radially polarized beam in a fiber rod to allow calculation of the required operating parameters, and to understand the benefits and limitations of this power-scaling scheme. The model assumes that pump power deposited is transversely uniform across the core, and that heat flow resulting from waste heat generated via the laser pumping cycle is purely radial. Under these assumptions and following the approach described in [15], the refractive index,  $n(r, z)$ , can be expressed as:

$$n(r, z) = n_0(z) - \frac{1}{2}n_g(z)r^2, \tag{1}$$

where  $n_0(z)$  is the refractive index at the center of the core and  $n_g(z)$  describes the radial variation in refractive index, which is assumed to have a purely parabolic ( $r^2$ ) dependence and is given by:

$$n_g(z) = n_{th}(z) + n_s. \tag{2}$$

Here,  $n_s$  is a ‘static’ contribution to take into account the possibility the core does not have perfectly flat index profile across the central region and  $n_{th}(z)$  is the contribution that arises from the heat generated in the core. For a uniform transverse pump deposition profile, it can be shown that:

$$n_{th}(z) = \frac{P_h(z) \, dn/dT}{2\pi r_1^2 \kappa}, \tag{3}$$

where  $P_h(z)$  is the heat deposited per unit length at position  $z$  along the fiber rod,  $dn/dT$  the temperature coefficient of refractive index for the core material,  $r_1$  the core radius, and  $\kappa$  is its thermal conductivity. The ray transfer matrix for a graded refractive index medium of this form is given by [18].

$$\begin{pmatrix} A & B \\ C & D \end{pmatrix} = \begin{pmatrix} \cos\left(z\sqrt{\frac{n_g}{n_0}}\right) & \frac{1}{\sqrt{n_0 n_g}} \sin\left(z\sqrt{\frac{n_g}{n_0}}\right) \\ -\sqrt{n_0 n_g} \sin\left(z\sqrt{\frac{n_g}{n_0}}\right) & \cos\left(z\sqrt{\frac{n_g}{n_0}}\right) \end{pmatrix}. \tag{4}$$

Using the above ray transfer matrix and applying the ABCD law [18], we can determine how a radially polarized beam evolves as it propagates through the TGFR for any given incident beam size and wavefront radius of curvature. If the pump deposition is uniform with distance  $z$  along the fiber rod and the incident beam forms a waist at the entrance to the fiber rod, then the beam radius,  $w(z)$ , as a function of distance is given by

$$w(z) = \sqrt{w_0^2 + \left(\frac{(M^2)^2 \lambda^2}{n_0 n_g \pi^2 w_0^2} - w_0^2\right) \sin^2\left(z\sqrt{\frac{n_g}{n_0}}\right)}. \tag{5}$$

The output beam radius from the fiber rod can be obtained from Eq. (5) by setting  $z$  equal to the fiber length. In deriving Eq. (5), ‘ $\lambda$ ’ is replaced by ‘ $M^2 \lambda$ ’ in the expression for the complex beam parameter to account for the higher beam propagation factor ( $M^2$ ) for a radially polarized beam compared to the fundamental mode. In general, the beam size varies in a sinusoidal manner with distance along the fiber rod, having a period of  $\pi\sqrt{n_0/n_g}$ . However, when

$$w_0 = \left(\frac{(M^2)^2 \lambda^2}{n_0 n_g \pi^2}\right)^{0.25}, \tag{6}$$

thermal guiding precisely balances diffraction and the beam size remains constant as it propagates along the fiber rod. In the situation where thermal guiding dominates over any static contribution (i.e.,  $n_{th} \gg n_s$ ), then the above condition for constant size beam propagation becomes:

$$w_0 = \left(\frac{2r_1^2 \kappa (M^2)^2 \lambda^2}{\pi n_0 P_h \, dn/dT}\right)^{0.25}. \tag{7}$$

This simple expression provides us with a starting design aid for TGFR lasers and amplifiers. The material parameters (i.e.,  $\kappa$ ,  $\frac{dn}{dT}$ ,  $n_0$ ) are fixed for a given host composition. However, the values for  $r_1$  and  $P_h$  can be adjusted through the fiber design, rare-earth ion doping concentration, pump power, and pump wavelength to achieve the desired outcome in terms of value for  $w_0$ . The goal of a much larger mode size and shorter fiber length than can be achieved in conventional double-clad fibers is quite straightforward to realize, but at the expense of a limited range of pump power for optimal performance and beam quality owing to the dependence of beam size on pump power. It is also worth mentioning that the ability to achieve a large thermally guided mode size is easier for higher-order modes and at longer operating wavelengths, as might be expected. Any deviation of the incident beam size from the value defined in Eq. (7) will result in a sinusoidal variation in beam size along the TGFR with a period:

$$\Delta z = \sqrt{\frac{2\pi^3 r_1^2 n_0 \kappa}{P_h \, dn/dT}}. \tag{8}$$

In reality,  $P_h$  is a function of  $z$  and decreases along the fiber rod approximately as

$$P_h \approx \alpha_p \gamma P_{pi} \exp(-\alpha_p z), \tag{9}$$

where  $P_{pi}$  is the launched (incident) pump power (assuming launching from one end),  $\gamma$  the fraction of absorbed pump power converted to heat, and  $\alpha_p$  is the absorption coefficient for pump light launched into the core (for core pumping) or inner cladding (for cladding pumping). This expression assumes negligible ground-state depletion. Providing that the pump absorption length,  $l_{abs} = 1/\alpha_p$ , is long compared to the period,  $\Delta z$ , then expressions (5)–(8) remain approximately valid with  $P_h$  defined as in Eq. (9). One issue with the TGFR now becomes apparent—there is a limit to the device length dictated by the need for sufficient heat load along the full length of the fiber rod. As  $P_h$  decreases along the fiber, the thermally guided beam size increases and eventually is no longer guided in the core resulting in multi-mode guiding by the step-index core guide and consequent degradation in beam quality. Thus, for a single-pass pumping configuration, the fiber rod length must be shorter than the length needed for efficient absorption of pump light at the expense of a decrease in overall efficiency. This can be remedied by recycling unabsorbed pump light for a second-pass of the fiber rod or employing a double-end pumping arrangement. In both cases, the fiber rod length can be selected to yield a relatively uniform thermal loading density along the entire length.

Figure 4 shows the calculated beam radius for a radially polarized beam with an  $M^2$  value of 2 as a function of distance,  $z$ , along the TGFR used in our experiments for several different scenarios. In each case, the fiber rod is 100 mm long and pump light from a fiber-coupled pump source at 915 nm is launched into the fiber rod at the signal output end (i.e., pump light is counter propagating with respect to the 1030 nm radially polarized seed). The fiber rod is cooled by direct thermal contact with an aluminum heat sink in a manner to ensure purely radial heat flow and the thermal conductivity of the core is taken to be that of silica (i.e.,  $1.38 \text{ W m}^{-1} \text{ K}^{-1}$  [19]) and the change of refractive index with temperature is taken to be  $12.9 \times 10^{-6} \text{ K}^{-1}$  [20].

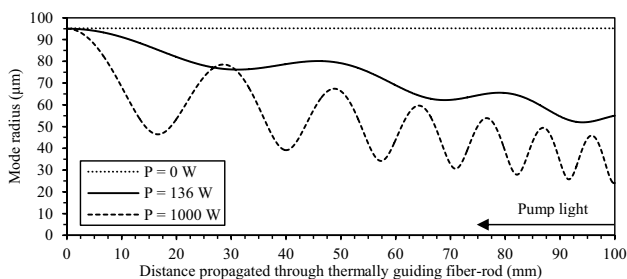


**Fig. 4** Calculated radially polarized beam radius with respect to propagation distance in the thermally guiding fiber rod. Pump light is introduced at  $z = 100$  mm counter propagating to the signal. Data are shown for input pump powers of 0 W, 136 W, and 1000 W

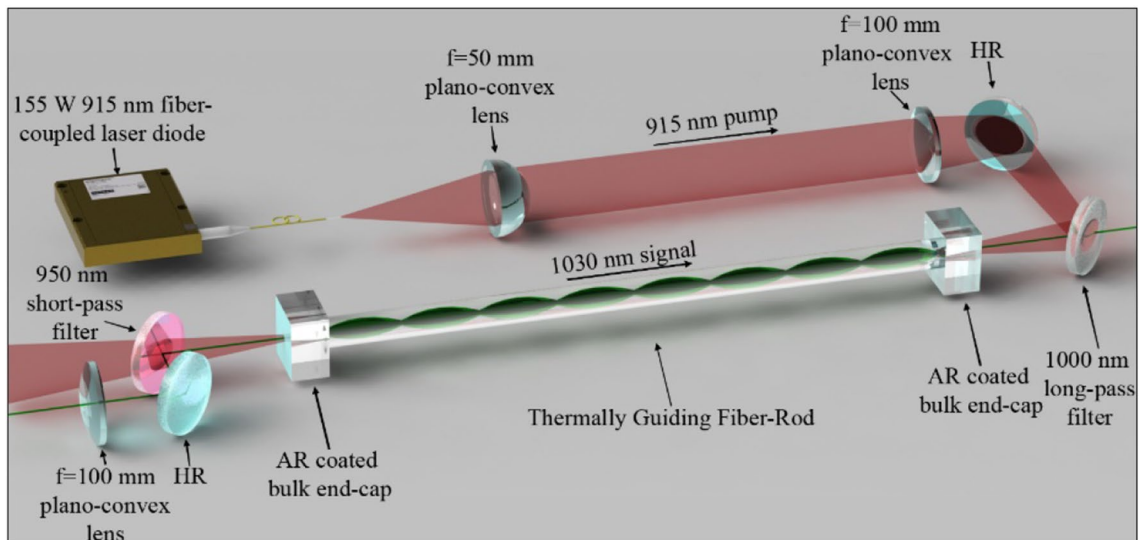
In the previous work [15], characterization of the fiber rod profile revealed an intrinsic (static), weakly guiding contribution to the core's refractive index profile. Without pumping, this yields a calculated beam waist radius (from Eq. (6)) at which guiding balances the diffraction of  $95 \mu\text{m}$ . This beam size was selected for the input beam as the beam size remains constant along the fiber rod (shown by the dotted line in Fig. 4), which simplifies alignment as no pump is required. The solid line in Fig. 4 shows the calculated beam radius through the fiber rod with an input beam waist of  $95 \mu\text{m}$  and the maximum measured pump power of 136 W available for our amplifier experiments. The beam radius has an overall tendency to decrease with propagation distance along the fiber rod due to the heat deposition density being higher at the pump input end. Oscillation of the beam radius as it propagates down the fiber rod is now evident, as expected, due to the interplay between diffraction and thermal lensing as the beam periodically diverges and focusses. The beam radius oscillates around a central value, which is determined by the power deposited as heat at a given axial position within the fiber rod core and can be found from Eq. (5). Most importantly, the model indicates that under the intended experimental conditions, the radially polarized beam is guided with a high average beam radius of  $\sim 73 \mu\text{m}$  and does not come close to interacting with the core–cladding interface at  $r_1 = 150 \mu\text{m}$ .

Figure 4 also shows the scenario with an input beam waist radius of  $95 \mu\text{m}$  and a much higher pump power of 1000 W (dashed line) to illustrate the power-scaling potential of the TGFR geometry. One can see that the average beam radius decreases to  $\sim 54 \mu\text{m}$  with the increase in heat load, and the amplitude of the oscillation of beam radius increases while the period decreases. However, the amplitude of oscillation may be decreased using a more appropriate choice of input beam waist, which can be estimated from Eq. (6). It is encouraging for future power scaling that the TGFR is predicted to guide a radially polarized seed even at these extreme pump powers with a relatively large beam size to help mitigate against damage and unwanted non-linear loss processes. Furthermore, the fiber rod design could be modified (e.g., by decreasing the Yb doping level) to reduce the thermal loading density and allow larger beam sizes.

## 4 Radially polarized seed amplification

Using insight gained from the thermal guidance model described in the previous section, amplification of the radially polarized output from the Yb:YAG laser described in Sect. 2 was investigated using the experimental arrangement illustrated in Fig. 5.

A 100 mm long sample of the Yb-doped triple-clad fiber was used in the amplifier setup. Fused silica end caps



**Fig. 5** Schematic of the thermally guiding fiber rod amplifier experiment. The 1030 nm radially polarized seed source was focused into the fiber rod at the calculated optimum beam radius of 95  $\mu\text{m}$ . Pump light was provided by a 155 W at 915 nm diode laser

(7 mm  $\times$  7 mm  $\times$  4 mm thick) with anti-reflection-coated outer faces at the pump and signal wavelengths were spliced to both ends of the fiber rod using a carbon dioxide laser to reduce feedback and loss. The fiber rod was then sandwiched in a two-part water-cooled aluminum heat sink to provide uniform cooling. The seed beam from the radially polarized Yb:YAG laser was coupled into the core with an arrangement of anti-reflection-coated plano-convex lenses and beam-steering mirrors to yield a beam waist at the interface between the input end cap and fiber rod with the desired beam radius of 95  $\mu\text{m}$ . Pump light was provided by a commercially available fiber-coupled pump diode (nLight, Inc.) with a maximum output power of 155 W at 915 nm. The output from the pump delivery fiber (105  $\mu\text{m}$  and 0.22 NA) was coupled into the opposite end of the fiber rod with the aid of a telescope comprising a 50 mm focal length plano-convex collimating lens and a 100 mm focal length plano-convex focusing lens to yield the optimum launch conditions.

Additionally, a 1000 nm long-pass filter was included in the output beam path to separate the amplified 1030 nm radially polarized output from the 915 nm pump light.

The radially polarized seed beam was guided through the core of the fiber rod in the absence of pump power due to the small static parabolic refractive index profile over the central portion of the core. As the pump power was increased, the output beam was observed to periodically focus and diverge from the output of the thermally guiding fiber rod, as predicted by the model. Figure 6a, b shows a comparison between CCD camera (Spiricon SP620U) images of the input radially polarized seed and the amplified output from the TGFR for a pump power of 136 W (launched). Before amplification, the beam had a near-perfect annular intensity profile, as expected for a radially polarized beam. After amplification in the TGFR, the same annular intensity profile is recovered with very slight distortion on one side believed to be due to slight misalignment. The  $M^2$  parameter

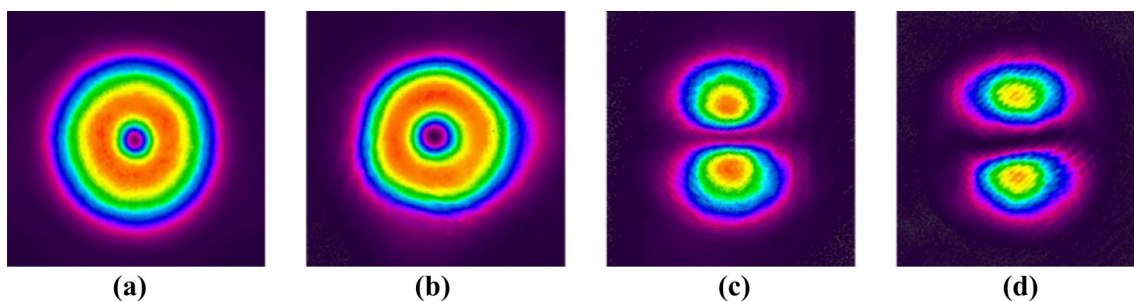


**Fig. 6** Intensity profiles for: **a** radially polarized seed, **b** amplified radially polarized beam, **c** radially polarized seed transmitted through linear polarizer, **d** amplified radially polarized beam transmitted through linear polarizer

of the amplified radially polarized beam was measured as  $2.1 \pm 0.1$ , and hence very slightly higher than for the seed source, but consistent with the slight degradation observed in Fig. 6b. These results confirm that the beam quality is largely preserved after the amplification over the full range of available pump power and, most importantly, there was no evidence of mode coupling and the dramatic degradation in beam quality that would be expected if the mode interacts with the core–cladding interface.

The preservation of the radial polarization purity is an important consideration in the performance of the TGFR amplifier. Figure 6c, d represents CCD camera images of the radially polarized mode after transmission through a linear polarizer, where Fig. 6d has been amplified. Figure 6c is symmetrical and exemplary of the expected remaining intensity distribution after a linear polarizer. The amplified intensity distribution in Fig. 6d shows a similar two-lobe intensity distribution albeit with a small amount of distortion present; however, there is no evidence of depolarization due to the amplification. To confirm this, the RPER of the amplified output beam at the maximum pump power was measured using the approach described earlier in Sect. 2 and was found unchanged at 100:1. This result confirms the postulation that radial polarization would be unaffected by detrimental thermally induced depolarization due to birefringence between radial and azimuthal components.

The combination of only a very slight measured decrease in beam quality and preservation of polarization purity by the TGFR amplifier suggest that this amplifier geometry has the potential to be scaled to higher power levels while retaining the unique features of radially polarized beams. To further assess the performance of the TGFR as an amplifier with respect to gain, the output power was measured over a range of incident pump powers for seed powers of 80 mW and 2.5 W (see Fig. 7). The TGFR yielded a maximum amplified output power 10.7 W for a seed power of 2.5 W with 54 W of absorbed pump power. This corresponds to a single-pass gain of 6.4 dB and an extraction efficiency of

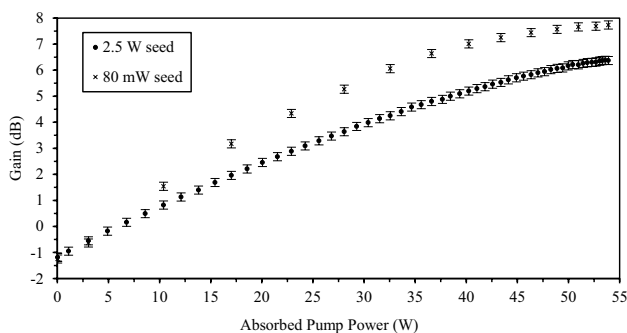


**Fig. 7** Measured gain for thermally guiding fiber rod amplifier as a function of absorbed pump power for launched seed powers of 80 mW and 2.5 W

20.6%. The maximum small-signal gain for a seed power of 80 mW was 7.7 dB. Figure 7 shows negative gain below an absorbed pump power of 6.7 W. This is the pump power required to reach transparency due to the quasi-three level Yb-doped silica having significant signal absorption.

Higher gain could, in principle, be achieved using a longer fiber rod to increase the pump absorption efficiency; however, in this study, the emphasis was directed toward the impact of the TGFR on beam quality and polarization purity. From Fig. 7, it is evident that there is a roll over in gain toward the highest pump power. This is believed to be due to amplified spontaneous emission (ASE) supported by the observation of a combined power of 5 W of broadband emission exiting the dichroic filters at both ends of the TGFR at the maximum pump power. While this represents only a small fraction of the power unaccounted for, it is likely that the total ASE power is much higher due to there being emission along closed paths that we are unable to access in our measurements. Clearly, the ability to scale to higher powers in an efficient manner will be dependent on identifying effective method for suppression of ASE without incurring significant loss for the pump and seed. One important aspect of the design will be to ensure that the radially polarized mode propagates with an average beam radius closer to the radius of the core to increase the overlap between seed and pump. In this way, the seed will preferentially saturate the gain helping to suppress ASE, as well as improve extraction efficiency. This could be achieved by, for example, employing a lower Yb doping level to reduce the thermal loading density for a given pump power. In addition, spatial filtering of the ASE should be possible in a multi-stage amplifier configuration; the ASE is primarily guided by the fiber waveguide and is, therefore, more divergent than the thermally guided radially polarized mode and, hence, can be removed between amplifier stages with strategically positioned apertures. There are a number of avenues that could be taken to scale power further, but the important prerequisite is an amplifier geometry that can preserve beam quality and polarization purity for radially polarized beams; we have shown that the TGFR is very promising in this regard.

## 5 Conclusion

In summary, amplification of a radially polarized beam using a thermally guiding fiber rod with a 300  $\mu\text{m}$  core diameter has been demonstrated. Mode quality and polarization were well preserved after amplification, with no measured loss in the polarization purity and only a small increase in the  $M^2$  parameter from  $1.9 \pm 0.1$  to  $2.1 \pm 0.1$ , which was attributed to imperfect alignment. The gain of the amplifier was measured for a range of absorbed pump powers reaching a value of 6.4 dB for a launched seed power of 2.5 W.

The corresponding maximum amplified output power was 10.7 W. A theoretical model for the thermal guidance was developed to allow for the calculation of beam radius of a higher-order mode as a function of propagation distance for a given input beam waist and pump power. The model suggests that scaling amplified powers to the kW level is feasible while retaining much larger mode sizes than are typical of conventional double-clad fibers. Our experiments revealed that ASE is likely to be a limiting factor on extraction efficiency and power scalability with the current fiber rod amplifier configuration. Therefore, further optimization of the design to improve the overlap of the signal with the gain region and employing multiple amplifier stages to allow spatial filtering of ASE between stages would be beneficial. This study has confirmed the benefits of the thermally guiding fiber rod geometry for amplifying axially symmetric beams, such as a radially polarized beam, with regard to its ability to preserve beam quality and polarization purity. Thus, improved designs targeted at further power scaling and suppression of ASE may open up the potential of power levels in the kW regime benefiting a range of applications.

**Supplementary material** The data underpinning this publication are available from the University of Southampton repository at <https://doi.org/10.5258/SOTON/D0962>.

**Acknowledgements** T. L. Jefferson-Brain and M. D. Burns acknowledge EPSRC (UK, Grant No. 1921150 & 1921199) for the provision of studentship support.

**Open Access** This article is distributed under the terms of the Creative Commons Attribution 4.0 International License (<http://creativecommons.org/licenses/by/4.0/>), which permits unrestricted use, distribution, and reproduction in any medium, provided you give appropriate credit to the original author(s) and the source, provide a link to the Creative Commons license, and indicate if changes were made.

## References

1. Y. Liu, D. Cline, P. He, Nucl. Instrum. Methods Phys. Res. **424**, 296 (1999)
2. L. Novotny, M.R. Beversluis, K.S. Youngworth, T.G. Brown, Phys. Rev. Lett. **86**, 5251 (2001)
3. V.G. Niziev, A.V. Nesterov, J. Phys. D **32**, 1455 (1999)
4. M. Meier, V. Romano, T. Feurer, Appl. Phys. A **86**(3), 329 (2007)
5. J.W. Kim, J.I. Mackenzie, J.R. Hayes, W.A. Clarkson, Opt. Express **19**, 14526 (2011)
6. K. Yonezawa, Y. Kozawa, S. Sato, Opt. Lett. **31**, 2151 (2006)
7. M.A. Ahmed, A. Voss, M.M. Vogel, T. Graf, Opt. Lett. **32**, 3272 (2007)
8. D. Lin, J.M.O. Daniel, M. Gecevičius, M. Beresna, P.G. Kazansky, W.A. Clarkson, Opt. Lett. **39**, 5359 (2014)
9. S.C. Tidwell, D.H. Ford, W.D. Kimura, Appl. Opt. **29**, 2234 (1990)
10. G. Machavariani, Y. Lumer, I. Moshe, A. Meir, S. Jackel, Opt. Commun. **281**, 732 (2008)
11. I. Moshe, S. Jackel, A. Meir, Opt. Lett. **28**, 807 (2003)
12. C.R. Smith, S.J. Beecher, J.I. Mackenzie, W.A. Clarkson, Appl. Phys. B **123**, 225 (2017)
13. M.A. Ahmed, M. Haefner, M. Vogel, C. Pruss, A. Voss, W. Osten, T. Graf, Opt. Express **19**, 5093 (2011)
14. M. Fridman, M. Nixon, M. Dubinskii, A.A. Friesem, N. Davidson, Opt. Lett. **35**, 1332 (2010)
15. C. Smith, N. Simakov, A. Hemming, W.A. Clarkson, Appl. Phys. B **125**(2), 32 (2019)
16. W. Koechner, *Solid-state laser engineering*, vol. 1 (Springer, New York, 2013)
17. G. Machavariani, Y. Lumer, I. Moshe, A. Meir, S. Jackel, N. Davidson, Appl. Opt. **46**, 3304 (2007)
18. H. Kogelnik, T. Li, Appl. Opt. **5**, 1550 (1966)
19. D.C. Brown, H.J. Hoffman, IEEE J. Quantum Electron. **37**(2), 207 (2001)
20. T. Toyoda, M. Yabe, J. Phys. D **16**(5), 97 (1983)

**Publisher's Note** Springer Nature remains neutral with regard to jurisdictional claims in published maps and institutional affiliations.